energies

MDPI

Article

Effect of Natural Ilmenite on the Solid Biomass Conversion of Inhomogeneous Fuels in Small-Scale Bubbling Fluidized Beds

Tanja Schneider *, Dominik Müller and Jürgen Karl

Chair of Energy Process Engineering, Department of Chemical and Biological Engineering, Friedrich-Alexander-Universität Erlangen-Nürnberg, Fürther Straße 244f, 90429 Nürnberg, Germany; dominik.mueller@fau.de (D.M.); juergen.karl@fau.de (J.K.)

* Correspondence: tanja.t.schneider@fau.de

Abstract: The application of oxygen carriers as alternative bed material in fluidized bed combustion originates from chemical lopping processes. They serve as oxygen transport agents undergoing consecutive redox cycles. Thereby, oxygen carriers can provide surplus oxygen in oxygen-lean areas of fluidized bed combustion processes. In turn, re-oxidation takes place in oxygen-rich reactor parts. A more homogeneous combustion and reduced CO emissions follow during steady-state operation. However, especially regarding solid biomass conversion, inhomogeneous fuel qualities result in transient combustion conditions. Therefore, this research deals with the influence of the oxygen carrier ilmenite on solid biomass conversion. Separated batch experiments with methane (volatile), char and wood pellets took place in a laboratory bubbling fluidized bed reactor. They reveal that ilmenite enhances the in-bed CO_2 yield by up to 63% during methane combustion. Batch char experiments confirm that solid–solid reactions with ilmenite are negligible. However, heterogeneous gas–solid reactions reduce the O_2 partial pressure and limit the char conversion rate. The batch wood pellet experiments show that the ilmenite oxygen buffering effect is mitigated due to high local oxygen demand around the pellets and limited pellet distribution in the bed. Finally, the continuous operation in a 100 kW_{th} BFB with inhomogeneous fuel input indicates a higher in-bed fuel conversion and confirms lower CO emissions and less fluctuation in the flue gas during inhomogeneous fuel supply.

Keywords: ilmenite; oxygen carrier; bubbling fluidized bed; oxygen carrier aided combustion; biomass

Citation: Schneider, T.; Müller, D.; Karl, J. Effect of Natural Ilmenite on the Solid Biomass Conversion of Inhomogeneous Fuels in Small-Scale Bubbling Fluidized Beds. *Energies* **2022**, *15*, 2747. https://doi.org/10.3390/en15082747

Academic Editor: Bruno Facchini

Received: 16 March 2022
Accepted: 7 April 2022
Published: 8 April 2022

1. Introduction

The decentralized application of solid biomass fuels can make an important contribution to the energy transition toward a CO_2 neutral energy supply. However, the thermochemical conversion of solid biomass often involves slagging and fouling issues due to the contained ash [1]. Inhomogeneous fuel qualities even intensify related problems. In general, fluidized bed combustion (FBC) plants address these issues; they provide increased fuel flexibility due to a homogeneous temperature distribution and the mitigation of hot spots. Large-scale FBC plants are state-of-the-art regarding the exploitation of biogenic residues and waste. Small-scale FBC solutions mostly fail due to low efficiencies, high emissions or unreasonably high operational efforts and fuel handling.

During recent years, the application of so-called oxygen carriers (OC) as alternative bed material in large-scale circulating fluidized beds (CFB) revealed further potential process optimization. Thunman et al. [2] introduced this process as oxygen carrier-aided combustion (OCAC). The substitution of the conventional silica sand bed material by an OC has its origin in the chemical looping process (CLC) [3,4]. According to CLC, the applied oxygen carrier undergoes reversible redox cycles in oxidizing and reducing atmospheres. Thereby, it can provide surplus oxygen in oxygen-lean areas for the reduction of fuels during combustion [5]. The main effects presented in the literature are the reduction in CO emissions (up to 80%) at nearly stoichiometric process conditions [2,6] as well as the

efficiency increase caused by the possible reduction in the excess air ratio [7]. However, these concepts are mainly based on CFB processes aiming at large-scale applications [7–9]. In terms of decentralized, small-scale solutions based on fluidized bed combustion, bubbling fluidized beds (BFB) are more suitable [10,11]. However, the process management of small-scale BFB generally differs from large-scale CFB; particle sizes increase, while fluid velocities decrease in BFB plants. Moreover, the high bed expansion in the gas phase of CFB processes results in low particle volume fractions. Furthermore, large-scale fluidized bed boilers mostly apply staged combustion. As a result, the gas compositions and reaction zones differ from single-stage combustion. Moreover, single-stage, small-scale BFB aims at a maximized heat release in the fluidized bed in order to realize heat extraction directly out of the fluidized bed [11–13]. All these variations affect the conversion of the ongoing oxygen carrier redox cycles and, consequently, the reactivity [14].

Some authors have already presented the transition of the OCAC process from large-scale CFB to small-scale BFB in a bubbling fluidized bed-fired CHP pilot plant [15]. The experiments in a field test environment confirmed a CO reduction of up to 75% during a steady-state operation with wood pellets. Recent experiments conducted by Hughes et al. [6,16] and Garcia et al. [17] confirmed the CO reduction potential using ilmenite as bed material for biomass-based fluidized bed combustion. Additionally, steady-state laboratory tests with methane demonstrated the local shift of oxygen within the BFB as well as an increased gaseous fuel conversion directly in the fluidized bed [18]. However, a discontinuous fuel input in partial load or highly inhomogeneous fuels are especially challenging in small-scale BFB. These are the main driving factors for incomplete burnout and varying excess air ratios. Consequently, CO emissions increase while efficiencies decrease [19].

Therefore, the following experiments examine the influence of transient combustion conditions on the enhancing effect of natural ilmenite during solid biomass OCAC. The thermochemical conversion of solid fuels comprises drying, devolatilization, gasification and combustion reactions. The particular influence of ilmenite on the fuel conversion during these phases is of special interest. The recent steady-state pilot plant and laboratory modeling experiments do not permit an isolated derivation of the mechanism and the interaction of ilmenite with the solid fuel until complete burnout in the BFB. Moreover, at unsteady combustion processes, not only a local but a temporal oxygen buffering effect by ilmenite becomes important.

The aim of this research is to define the effect of ilmenite on the combustion process of woody biomass in a BFB during OCAC. Hence, separated batch tests with discontinuous methane, char and wood pellet input in a lab-scale BFB serve to study the main affected processes during thermochemical conversion. The results are mainly discussed regarding the surplus oxygen provided in the BFB, the in-bed fuel conversion and the CO emissions. Moreover, they serve to define the time-dependent impact of ilmenite on the thermochemical conversion of wood pellets. Finally, the transfer of the determined effects to a 100 kW_{th} BFB unit follows.

2. Theory

In general, the thermochemical conversion of solid biomass can be separated into these subsequent main steps: drying of the solid; pyrolysis; and, finally, oxidation and gasification reactions of the emerged products. The main resulting components of solid biomass after drying and pyrolysis are steam, volatile matter, tars and remaining char (see Equation (1)). The drying and devolatilization are temperature-induced processes. When over stoichiometric conditions, the volatile matter, tars and the solid carbon contained in the char undergo further oxidation reactions (see Equations (2) and (3)).

$$\text{solid biomass} + \text{heat} \rightarrow \text{char (C + ash)} + \text{volatile matter } (H_2, CO, CH_4, C_xH_y) + \text{tars} + H_2O \quad (1)$$

$$\text{volatile matter } (H_2, CO, CH_4, C_xH_y) + O_2 \rightarrow CO_2 + H_2O \quad (2)$$

$$C\ (char) + O_2 \rightarrow CO + \frac{1}{2} O_2 \rightarrow CO_2 \quad (3)$$

The combustion of woody biomass is a widely discussed issue in the literature [20,21]. Therefore, the following covers only a brief overview of the most important interrelations. First, solid drying and pyrolysis take place. The drying process mainly depends on the structure and size of the particles. Diffusion and heat transfer processes are the rate-depending steps. The same applies for pyrolysis [22]. Reschmeier et al. [23] examined the pyrolysis kinetics of 6 mm wood pellets in a laboratory BFB and revealed the full conversion to char after approx. 40–50 s (800 °C). The remaining char covers approx. 10–15 wt% of the initial pellet mass [24], which is confirmed by Neves et al. [25]. However, in general, the composition of woody biomass covers a wide range and the fixed carbon content can reach even 25 wt% [26]. In general, CO is the main pyrolysis gas product followed by CO_2 and CH_4 at 800 °C [25].

Separately, char conversion is the focus of several research activities. The main product leaving the boundary layer of char particles in a fluidized bed combustion at moderate temperatures is CO_2. CO is the subordinated gas species, while higher temperatures favor the increase in the CO/CO_2 ratio [27]. The resulting CO/CO_2 ratio leaving the char particles at around 800 °C ranges in the literature between 0.1–0.25 [28,29] and 0.5 [30]. In particular, the origin of the char affects the resulting CO/CO_2 ratio [31,32]. The boundary layer diffusion of oxygen and the product diffusion of CO and CO_2 are seen to be the rate-controlling steps during combustion within a temperature range of 800–900 °C [33]. Sadhukhan et al. [34] observed in their experiments with 0.92 to 6 mm coal particles that, besides the particle size and bed temperature, the available oxygen content in the gas phase influences the char conversion. This has been confirmed by Hesketh et al. [35] who studied the influence of the presence of volatiles on the char conversion in a FBC. The reaction kinetics prefer the homogeneous gas phase reaction of oxygen with volatiles in contrast to the heterogeneous gas–solid reaction. This decreases the available oxygen for the char conversion and prolongs the burnout time. With regard to the combustion of the volatiles, similarly, a higher oxygen content raises the reaction rate while the mainly temperature-driven devolatilization is not affected [36].

Figure 1 schematically summarizes the described steps for the combustion of wood pellets at 800 °C with air. The qualitative illustration of the change in particle mass over time is based on the literature results presented previously. Its intention is to emphasize the discontinuous theoretical oxygen demand. It additionally includes the theoretically provided oxygen over time as a continuous O_2 mass flow. This highlights the increasing discrepancy in the theoretical oxygen consumption. Simultaneously, the composition of released product gases changes in a time-dependent manner.

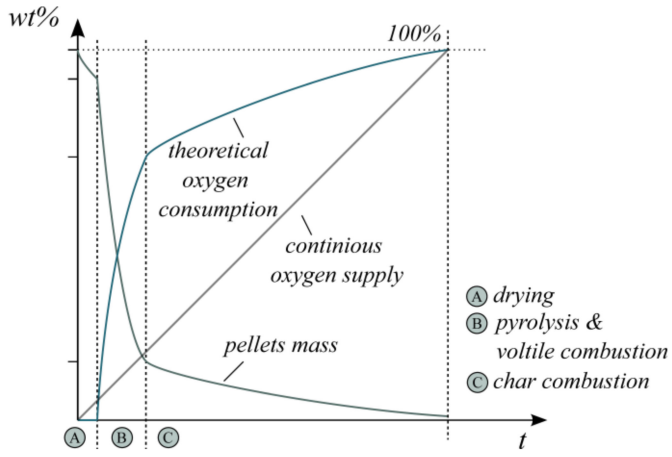

Figure 1. Schematic illustration of the pellet mass, theoretical oxygen consumption and oxygen supply during wood pellet combustion.

In reality, the process steps do not take place one after the other but overlay in some periods. This effect can be originated, for instance, by discontinuous fuel supply or inhomogeneous fuel composition. In general, the highest oxygen demand arises during volatile combustion, which covers only 10–30% of the overall time period for complete combustion [37,38]. Hence, an already slightly discontinuous fuel input (>10 s) may influence the oxygen balance in the flue gas. Moreover, this transient oxygen demand can result in varying flue gas compositions and involves the risk of unburnt hydrocarbons.

During OCAC, additional reactions involving the solid oxygen carrier take place and can influence the process steps previously described. The applied oxygen carrier in this research is natural ilmenite, which is also widely used in large-scale CFB OCAC [6,39–41]. Ilmenite ($FeTiO_3$) benefits from good availability, low cost and non-toxic properties. However, reversible redox cycles in CLC have revealed relatively low reactivity compared to other OCs. In general, the oxidation of ilmenite takes place in oxygen-rich combustion zones. The previous application of ilmenite in OCAC processes confirmed the formation of separated iron and titanium phases (see Equation (4)) [42]. Accordingly, moderate temperatures (<800 °C) favor a continuous increase in this iron-enriched phase hematite (Fe_2O_3) [43]. The subsequent reduction with gaseous fuels takes place in reducing atmospheres. The presence of CO_2 during OCAC inhibits the reversible reduction of the emerged Fe_2O_3 to FeO (wüstite). Therefore, the oxygen carrier usually reacts only to Fe_3O_4 (magnetite) (see Equations (5)–(7)) [4]. Overall, the reactivity of the reduction of Fe_2O_3 to Fe_3O_4 decreases, starting from H_2, CO toward CH_4 [44].

Oxidation in zones with an excess of oxygen:

$$2\,FeTiO_3 + \frac{1}{2}\,O_2 \rightarrow Fe_2O_3 \cdot TiO_2 + TiO_2 \rightarrow Fe_2O_3 + 2\,TiO_2 \quad (4)$$

Reduction in zones with a deficit of oxygen:

$$12\,Fe_2O_3 + 3\,CH_4 \rightarrow 8\,Fe_3O_4 + 2\,CH_4 + CO_2 + 2\,H_2O \rightarrow 24\,FeO + 3\,CO_2 + 6\,H_2O \quad (5)$$

$$3\,Fe_2O_3 + 3\,CO \rightarrow 2\,Fe_3O_4 + 2\,CO + CO_2 \rightarrow 6\,FeO + 3\,CO_2 \quad (6)$$

$$3\,Fe_2O_3 + 3\,H_2 \rightarrow 2\,Fe_2O_3 + H_2 + 2\,H_2O \rightarrow 6\,FeO + 3\,H_2O \quad (7)$$

Finally, during the OCAC of solid biomass, all named reactions (Equations (1)–(7)) overlap in the fluidized bed. Thus, previous mechanisms for solid biomass combustion in BFB have to be extended by the interaction with the oxygen carrier. The drying and pyrolysis processes are mainly diffusion and heat transfer driven processes. Hence, the oxygen transport capacity of the OC should have no direct influence during these steps. In general, the heat transfer in fluidized beds is quite good and, therefore, small deviations in the physical properties of the OC, e.g., the heat transfer coefficient or heat capacity, should only have a minor effect on the heating rate of the solid fuel. Thus, in the following, these effects are neglected.

Moreover, the literature indicates that solid–solid reactions between the oxygen carrier and a solid fuel only become significant with close and long-lasting contact between both [45]. The prevailing circumstances in FBC inhibit this possible reaction path [46]. Therefore, the application of solid fuels in the fuel reactor of CLC processes is normally combined with in situ gasification of the solids [4,47].

However, the presence of an OC can affect the combustion of the volatiles (see Equations (5)–(7)) as well as indirectly affecting the char conversion. Moreover, the discontinuous oxygen demand during woody biomass combustion (see Figure 1) can mitigate the complete burnout of the volatiles. The temporal oxygen buffering ability of the OC can provide surplus oxygen for a limited period and thereby reduce emerging unburnt hydrocarbons. On the contrary, the re-oxidation of the OC reduces the available oxygen content in the gas phase (see Equation (4)). This reduction of the O_2 partial pressure can

consequently affect the char burnout rate in a similar manner. Finally, this would result in a higher average char inventory during operation in the BFB.

Thus, this research first separately examines the volatile and char combustion with ilmenite in the laboratory BFB model reactor. Afterward, the discontinuous combustion of wood pellets combines both processes. As a result, the qualitative combustion schematic depicted in Figure 1 can be updated for the BFB combustion with ilmenite, as shown later in Figure 11. Finally, the enhancing effects during OCAC are transferred to continuous operation with an inhomogeneous fuel supply in a 100 kW_{th} BFB unit.

3. Materials and Methods

3.1. Measurement Setups

The presented experiments were performed in two different setups: a laboratory BFB model reactor (see Figure 2a) and a 100 kW_{th} scale-up BFB reactor (see Figure 2b). The laboratory BFB model reactor had a diameter d_{FB} of 100 mm and a length of 645 mm. The fluidization medium, either air or pure nitrogen, enters the BFB reactor through the airbox and a plate with air nozzles. The open reactor setup enables the fuel dosage from the top. Gaseous fuels enter the BFB through a fuel distribution probe. The distributed injection to the BFB took place at a reactor height of 90 mm. Solid fuel particles enter the reactor from the top and fall on the BFB surface. An electrical bed heater controls the FB temperature measured by a thermocouple type K. The double-walled cooled gas sampling probe is adjustable along the reactor height and allows flexible gas analysis of the product gas.

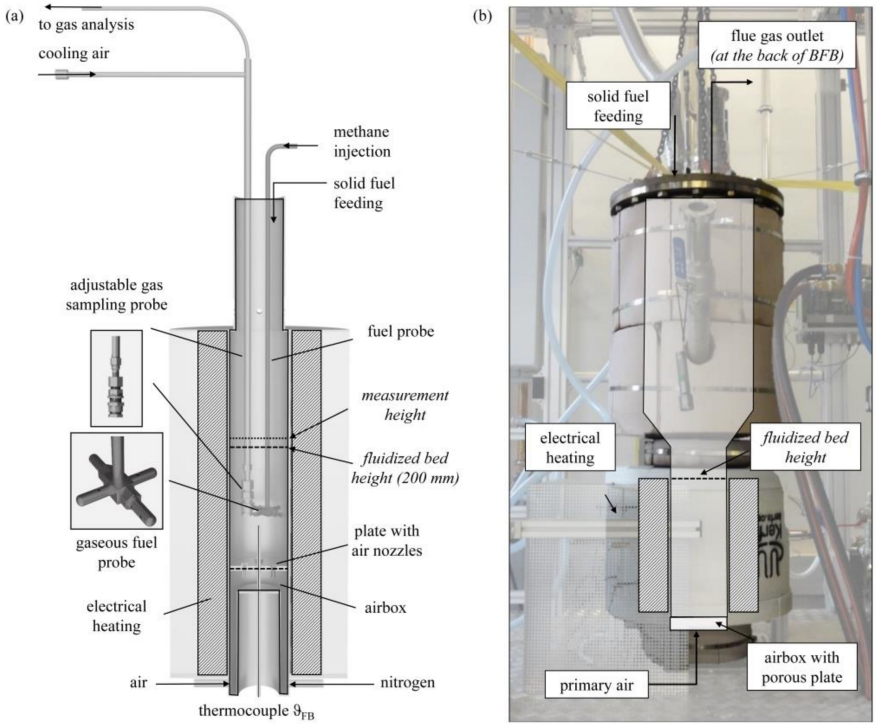

Figure 2. Setup of (**a**) laboratory BFB model reactor for the injection of methane (to simulate "volatiles" combustion) and solid wood and char pellets (measurement series 1–4) and (**b**) 100 kW_{th} BFB unit for the experiments with discontinuous solid fuel feed (measurement series 5).

The 100 kW_{th} scale-up BFB reactor had a diameter of d_{FB} = 200 mm and a height of 400 mm, with a conical freeboard extension to a diameter of 400 mm. The overall reactor height was 1600 mm. An electrical heating system (9 kW) covers the freeboard region and regulates the fluidized bed temperature during operation. An electrical air preheater (4 kW) realizes the preheating of the combustion air, which enters the reactor via a porous plate. An automated screw conveyor system doses the solid fuels from the reactor top. The measurement of the flue gas composition takes place at the reactor outlet.

For both setups, ABB AO2020 gas analyzers measured the resulting product gas composition. The integrated measurement modules determined the concentration of O_2 (0–21 vol.-%), H_2 (0–100 vol.-%), CH_4 (0–60 vol.-%), CO_2 (0–100 vol.-%) and CO (0–30 vol.-%). A second gas analyzer with adopted measurement ranges additionally identified the concentration of CO_2 (0–20 vol.-%) and CO (0–3000 ppm). During transient combustion of the wood pellets, an upstream wash bottle was necessary to eliminate potential tars in the product gas. Moreover, a NO_x sensor (Bosch EGS-NX) in the flue gas outlet measured the O_x and NO_x content.

3.2. Applied Materials

Two different bed materials served for the fluidized bed experiments. The inert silica sand HR0.1–0.6 T originated from Amberger Kaolinwerke Eduard Kick GmbH and had a purity of SiO_2 > 98.0 wt%. The applied natural ilmenite from Titania A/S served as the oxygen carrier bed material. Both belong to Geldart group B [48]. While the silica sand material has a lower solid density ρ_s, the particle size distribution reveals higher particle sizes compared to ilmenite. Thereby, the minimal fluidization velocities u_{mf} measured at 20 °C were similar (see Table 1).

Table 1. Properties of used bed materials. (adapted with permission from [18]. Copyright 2021 American Chemical Society.)

Material	Solid Density ρ_S (kg/m^3) [1]	Sauter Mean Diameter d_{32} (µm) [2]	Porosity ε_{mf} (-) [2]	Fluidization Velocity u_{mf} (at 20 °C) (m/s) [2]
Silica sand	2650	413	0.429	0.099
Ilmenite	3566	330	0.452	0.104

[1] According to manufacturer specification. [2] Own analysis.

The phase composition of the natural ilmenite reveals that only 62.33 wt% covered the active phase ilmenite ($FeTiO_3$). Additionally, the material shows smaller proportions of hematite (Fe_2O_3, 6.95 wt%) and minor magnetite (Fe_3O_4, 0.38 wt%) as well as rutile (TiO_2, 0.21 wt%). Other inert phases, mainly plagioclase and orthopyroxene, comprise almost one-third (30.13 wt%) of the natural material. Thus, the applied term *ilmenite* always refers to the complete material composition. For the applied natural ilmenite material, the initial oxygen transport capacity comprises theoretically max. 3.3 wt%. As already mentioned, moderate combustion temperatures favor the transition to a Fe_2O_3/Fe_3O_4-system, which further reduces the maximal oxygen transport capacity of the applied material 1.3 wt%.

The used gaseous fuel was comprised of bottled methane (>99.5%). The solid fuels covered certified wood pellets (ENplus A1 ISO 17225-2) as well as char pellets (see Figure 3). These were pelletized from char residues remaining in a biomass downdraft gasifier (Burkhardt GmbH, Mühlhausen, Germany) and only covered a minor proportion of volatile matter (see Table 2). Consequently, they could serve as fuel for the experimental simulation of the char combustion of solid biomass.

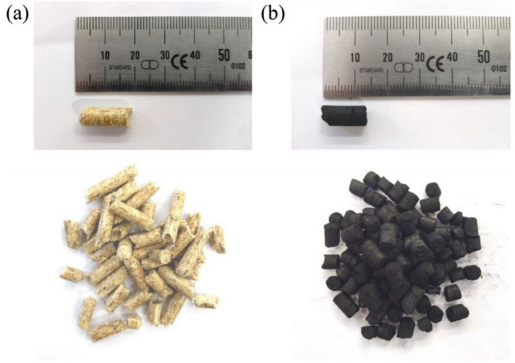

Figure 3. Samples of (**a**) wood pellets (measurement series no. 3–5) and (**b**) char pellets (measurement series no. 2).

Table 2. Properties of wood and char pellets used in measurement series no. 2–5.

Property	Wood Pellets	Char Pellets	Unit
Pellet diameter	6	6	mm
Carbon content (dry fuel)	50.4	85.5	wt%
Oxygen content (dry fuel) [1]	42.5	3.8	wt%
Hydrogen content (dry fuel)	6.2	0.4	wt%
Ash content (dry fuel)	0.7	10.3	wt%
Moisture content (as received)	7.8	30.0	wt%
Volatile substances (dry fuel)	83.3	7.1	wt%
Net calorific value	18.6	20.1	MJ/kg
Stoichiometric air demand	5.6	6.8	kg/kg

[1] Calculated according to DIN 51733:2016-04.

3.3. Measurement Procedure

The batch experiments were carried out in the presented BFB laboratory model reactor in order to define the influence of ilmenite on the particular combustion steps. The measurement series with inert silica sand as bed material served as the reference. The initial bed height for both bed materials was 200 mm in the reactor. Due to the different solid densities, the bed material mass in the reactor differed; 2.34 kg silica sand corresponded to 3.56 kg ilmenite. During each reactor heat-up with air, pre-oxidation of the fresh bed material ilmenite took place. Thereby, at the beginning of each measurement and in between each measurement series, ilmenite was fully oxidized.

The first experiments focused on the influence of ilmenite on the combustion of the volatiles (see Table 3, measurement series no. 1). Methane served as representative of the volatile matter. Methane injection to the BFB took place via the fuel probe at 90 mm BFB height. This simulated the devolatilization of pellets mixed randomly into the fluidized bed. The primary air volume flow maintained a constant fluidization velocity ($u/u_{mf} = 2.5$), while the methane injection was transient. For this purpose, the methane injection turns on for 10 s and subsequently pauses for 20 s. This sequence was repeated five times. Thereby, one measurement covered five overlaying oxidation/reduction exclusive oxidation cycles, respectively. This procedure was repeated for different fuel inputs covering the excess air ratios $\lambda = 0.5$, 0.75 and 1.0 during the 10 s of fuel input. With regard to the entire cycle (10 s air and fuel dosage +20 s only air dosage), the overall cycle excess air ratio increased to $\lambda_c = 1.5$, 2.25 and 3.0.

Table 3. Parameters of measurement series ($\vartheta_{FB} = 800$ °C).

No.	Reactor Unit	Fuel	Mass Silica Sand/Ilmenite (kg)	Fluidization Velocity u/u_0 (-)	Overall Cycle Excess Air Ratio λ_c (-)	Fuel Input [1]
1	Laboratory BFB	Methane	2.34/3.56	2.5	1.5/2.25/3.0	Transient: 10 s on, 20 s off; ~0.51/0.34/0.25 kW; 5 cycles
2	Laboratory BFB	Char pellets	2.34/3.56	2.5	4.7	Singular batch: 10 g char pellets, 20 min off; ~0.17 kW; 1 cycle
3	Laboratory BFB	Wood pellets	2.34/3.56	2.5	4.1	Repeated single pellet à 0.7 g, 1 min off; ~0.22 kW; 10 cycles
4	Laboratory BFB	Wood pellets	2.34/3.56	2.5	2.9	Repeated batch: 10 g wood pellets, 10 min off; ~0.31 kW; 3 cycles
5	100 kW_{th} BFB unit	Wood pellets	14.2/21.6	8.5	1.3/1.5/1.7/2.0	Transient: cycle times 5/20/40/60 s; ~8.5/7.5/6.5/5.5 kW; continuous operation

[1] Uncertainty of supplied fuel mass: +/−10 wt%.

In the same setup, measurement series no. 2 took place for studying the char combustion. Again, the fluidization with air remained constant during the entire experiment. In contrast, the fuel input (10 g char pellets, uncertainty +/−10%) was realized from the top of the open reactor and only took place once. In order to calculate the overall excess air ratio, the assumed cycle time for the complete oxidation of the char pellets was set to 20 min. This value was based on the measured burnout time in silica sand (see Section 4.1.2) and, therefore, was used also for the evaluation of ilmenite experiments. It resulted in a relatively high overall excess air ratio of $\lambda_c = 4.7$.

Finally, wood pellets served as solid fuel in measurement series no. 3 and no. 4. The fuel dosage from the reactor top covered the supply of single wood pellets à 0.7 g (uncertainty +/−10%) every 60 s. The resulting theoretical excess air ratio at the beginning of the cycle was approx. 1.5 but increased during the required cycle time for the complete combustion of the pellets to $\lambda_c = 4.1$ overall. The batch-wise dosage of 10 g wood pellets (uncertainty +/−10%, measurement series no. 4) followed, which resulted in temporary sub-stoichiometric conditions at the beginning of each cycle. This batch fuel dosage was repeated three times every 10 min, resulting in an overall excess air ratio of $\lambda_c = 2.85$ for an almost complete combustion of the pellets. To emphasize the transient combustion conditions, the authors added the theoretical oxygen content in the flue gas at instant full conversion qualitatively to the resulting diagrams (O_2 theo. at full conversion). This estimation has to be seen as a qualitative trend only and is based on pyrolysis and char oxidation kinetics from the literature [49,50].

For all measurements in the laboratory BFB, the measurement procedure took place several times to ensure reproducibility. The presented gas profiles were each exemplary impulse responses after the repeated fuel input.

The transfer of the batch experiments to continuous operation took place during automated operation in a 100 kW_{th} BFB unit. The necessary bed inventory was raised to 14.2 kg silica sand, which was 21.6 kg ilmenite, respectively. Measurement series no. 5 includes several experiments at different overall excess air ratios. This variation is a result of the variation of the fuel mass flow, while the primary air keeps constant for all measurements again. In order to examine the influence of an increasingly transient fuel input, at each excess air ratio, the fuel input cycle time varied. Short fuel input cycles imply almost continuous fuel feeding, while higher cycle times result in incrementally transient fuel supply. Table 4 summarizes the share of fuel dosage time of the screw conveyor depending on the excess air ratio. The proportional fuel dosage time was kept constant for all cycle times. Thus, the absolute fuel dosage time constantly increased.

Table 4. Share of fuel dosage time depending on the excess air ratio.

	Share of Fuel Dosage (-)			
Overall Cycle Time (s)	**λ_c = 1.3**	**λ_c = 1.5**	**λ_c = 1.7**	**λ_c = 2.0**
5/20/40/60	0.31	0.26	0.22	0.17

3.4. Data Evaluation

The evaluation and balancing of the gas composition in the BFB reactors used the nitrogen mass flow of the fluidization medium as inert tracer gas. Moreover, different calculable parameters served as an indicator for the comparison of silica sand combustion and ilmenite OCAC. For instance, the CO_2 yield γ_{CO2} considered the molar flow of produced CO_2 $\dot{n}_{CO_2,out}$ at the measurement point in relation to the introduced molar carbon $\dot{n}_{C_{in}}$.

$$\gamma_{CO_2} = \frac{\dot{n}_{CO_2,out}}{\dot{n}_{C,in}} \quad (8)$$

Usually, the oxygen transport capacity serves as an indicator to evaluate the enhancing effect of ilmenite in CLC processes. However, not all measurement setups permit the determination of the lower reduced state of the OC, which is necessary for the evaluation of

an average oxidation state of the OC. Therefore, the authors introduced a new parameter for evaluation: the specific provided oxygen mass $\dot{m}_{O_2}$ supplied by the OC (see Equation (9)). This determines the surplus provided oxygen by ilmenite based on the difference of the overall consumed oxygen during combustion with silica sand $\Delta m_{O_2,comb,sand}$ and with ilmenite $\Delta m_{O_2,comb,ilm}$. The division by the used ilmenite mass m_{ilm} and the cycle time t_c helps to compare results from different measurement series.

$$\dot{m}_{O_2} = \frac{\Delta m_{O_2,comb,ilm} - \Delta m_{O_2,comb,sand}}{m_{ilm} \cdot t_c} \quad (9)$$

4. Results

This section may be divided by subheadings. It should provide a concise and precise description of the experimental results, their interpretation, as well as the experimental conclusions that can be drawn.

4.1. Effect of Ilmenite on Separated Combustion Process Steps

4.1.1. Transient Methane Combustion with Ilmenite

First, focus is on the combustion of the volatile matter. This process covers only a short time period with regard to the whole pellet combustion duration (see Figure 1) but requires a large proportion of the total oxygen demand. Therefore, oxygen-lean combustion atmospheres can result in low overall excess air ratios. The experiments reflect this situation by the impulse addition of methane at temporarily sub-stoichiometric conditions (excess air ratios λ = 0.5, 0.75 and 1.0; see measurement series no. 1). Thereby, alternating oxygen-rich and oxygen-lean combustion atmospheres arise. The overall excess air ratios for a whole cycle increase (λ_c = 1.5, 2.25 and 3.0) as the oxidation periods balance the periods of overlaid air and methane dosage.

Figure 4 shows the resulting dry gas composition at the fluidized bed surface for the pulsed methane injection with silica sand (a) and ilmenite (b) as bed material. In general, the O_2 concentration decreases at lower excess air ratios. The CO_2 concentration behaves in the opposite manner. However, during fuel injection at sub-stoichiometric conditions, the whole oxygen should be theoretically consumed. Therefore, the diagram schematically depicts the theoretical oxygen content at full conversion (O_2 theo. at full conversion, see Experimental). It is obvious, that the gas analyzer softens the gas concentration profiles, especially the peaks. The reasons for that are back mixing effects and delays in the sampling probe tube and analyzer unit. However, this circumstance does not affect the measured amount of converted oxygen and fuel. Moreover, the measurements of the gas profiles take place directly above the BFB surface. Thus, incomplete conversion of the volatiles is quite possible.

As discussed comprehensively in Schneider et al. [18], steady-state methane feed results in a very low methane conversion in a fluidized bed due to absent air and methane preheating, limited reactant mixing in the setup and limited residence time in the BFB laboratory reactor. Nearly full conversion takes place above the BFB in the freeboard only.

A particularly important indicator for the in-bed fuel conversion is the CO_2-yield of the gas samples extracted from the freeboard. The low methane conversion limits the in-bed CO_2-yield to 13.0%, especially during the experiments with silica sand (see Table 5).

Contrarily, ilmenite experiments reveal that the OC can balance insufficient mixing in the fluidized bed and provide bounded oxygen for the conversion of methane. Thereby, the CO_2 yield reaches 80.3% at stoichiometric conditions. At high sub-stoichiometric conditions, the CO_2 yield even slightly exceeds the theoretically achievable values (see Table 5). Furthermore, after several cycles, the yield does not decrease, which indicates that there is still sufficient bounded oxygen in the ilmenite material available to buffer sub-stoichiometric conditions. The maximum theoretically bounded oxygen by the applied ilmenite mass is 117 g, while one methane injection cycle at λ = 0.5 requires only 0.9% of

this bound oxygen. Hence, ilmenite can buffer sub-stoichiometric conditions temporarily. For inert silica sand experiments, no comparable behavior is apparent.

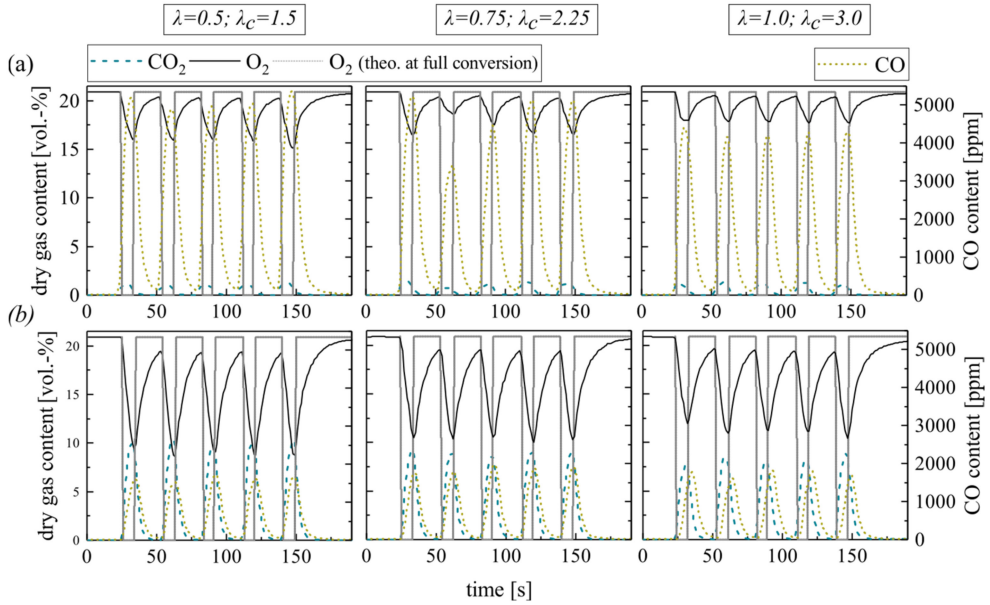

Figure 4. Dry gas composition measured at the fluidized bed surface depending on the excess air ratio for (**a**) silica sand and (**b**) ilmenite with methane as fuel (measurement series no. 1).

Table 5. In-bed CO_2 yield γ_{CO2} for silica sand and ilmenite as well as specific provided O_2 mass by ilmenite with methane as fuel depending on the excess air ratio λ (respectively, cycle excess air ratio λ_c) during fuel injection (measurement series no. 1).

		λ = 0.5 (λ_c = 1.5)	**λ = 0.75 (λ_c = 2.25)**	**λ = 1 (λ_c = 3.0)**
CO_2 yield (%)	Theoretical max	50.0	75.0	100.0
	Silica sand	7.0	10.4	13.0
	Ilmenite	52.4	66.6	80.3
Provided O_2 mass (g_{O2}/h per $kg_{ilmenite}$)	Silica sand	-	-	-
	Ilmenite	13.3	12.0	12.1

The different trends in the emerging CO concentration support the previous argumentation; higher CO concentrations at the silica sand BFB surface indicate an incomplete methane oxidation. In the ilmenite BFB, carbon monoxide is mainly oxidized to CO_2. The reason for this lies within the high reactivity of ilmenite toward CO compared to CH_4. Ilmenite reacts directly with arising CO emerging from incomplete homogeneous gas phase methane oxidation, while the direct oxidation of CH_4 is less dominating. Hence, the arising CO concentration only slightly varies at varying excess air ratios with ilmenite.

Finally, comparing silica sand and ilmenite experiments illustrates the specific oxygen mass $\dot{m}_{O_2}$ provided by the OC (see Table 5). The values keep almost constant, independent of the applied excess air ratio. Therefore, the authors suggest that the residence time of injected methane, i.e., reaction kinetics and diffusion processes, limit the heterogeneous gas–solid reactions with ilmenite. Hence, the higher oxygen supply due to transient conditions is limited, although complete re-oxidation of the OC takes place in between the fuel injection.

A comparison with previous results obtained in the same setup during steady-state conditions [18] reveals that the achieved in-bed CO_2 yield during transient conditions increases by 26.4% (λ = 0.75) and 41.2% (λ = 1.0). In contrast, the specific provided oxygen mass seems to be significantly lower. The reason for that is the reference of the specific

provided oxygen mass to the cycle time, i.e., 10 s air and fuel dosage + 20 s only air dosage. Relating the absolute provided oxygen mass only to the fuel dosage time (10 s) triples the specific provided oxygen. After that, the results are comparable at λ = 0.75, while the specific provided oxygen during transient stoichiometric conditions (λ = 1.0) exceeds the value achieved with steady-state conditions. This confirms the temporal buffering effect of ilmenite, but simultaneously emphasizes the prevailing limitations at lower excess air ratios due to residence time and reaction kinetics.

Finally, the experiments reveal that ilmenite enhances the in-bed conversion of gaseous fuels not only at steady-state but also transient conditions. Ilmenite provides a local and temporal shift of oxygen, enhances the in-bed CO_2 yield and efficiently mitigates arising CO emissions. Higher in-bed fuel conversions simultaneously result in a higher fluidized bed temperature increase during fuel injection. Consequently, the heat release in the BFB increases, as already shown by Müller [51].

4.1.2. Batch Char Combustion with Ilmenite

Beside the combustion of volatiles, char combustion is a governing reaction during the conversion of woody biomass fuels (see Figure 1). In the laboratory BFB, this process is reproduced by the batch combustion of char pellets. As known from CLC, ilmenite should not undergo a solid–solid reaction with the supplied char pellets [45]. In order to verify this assumption, fully oxidized ilmenite was fluidized with inert nitrogen during the supply of 10 g char pellets (see Figure 5). Except for a small CO and CO_2 peak, representing the remaining volatiles in the pellets, the gas profiles show no significant carbon conversion. After 15 min, the fluidization medium changes to air. Directly after, char conversion is initiated. This confirms that ilmenite mainly undergoes heterogeneous gas–solid reactions with the gaseous products from solid biomass conversion and shows no relevant reaction with solid char.

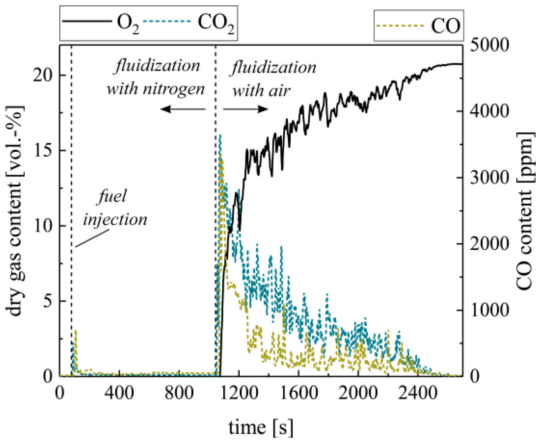

Figure 5. Dry gas composition measured at the ilmenite fluidized bed surface with char pellets as fuel during alternating fluidization mediums (N_2 and air).

Although ilmenite does not undergo a solid–solid reaction with biomass char, the presence of the OC can affect the char conversion during combustion. Therefore, Figure 6 compares the response of the dry gas concentration on the batch dosage of 10 g char pellets for silica sand (a) and ilmenite (b). In particular, the fluctuations in the gas profiles measured right above the fluidized bed surface differ. Further measurements of the gas concentrations directly in the FB confirm this behavior. Simultaneously, unsteady flame formation and extinction are apparent at the BFB surface during the silica sand experiment, which leads to an unsteady burnout. Obviously, ilmenite smoothens the oxygen consumption as well as the CO_2 and CO formation by a more homogeneous oxygen supply and, consequently, less flame formation on the bed surface. In line with that, ilmenite reduces the level of CO leaving the BFB and enhances in-bed fuel conversion. However, the time until full conversion of the supplied fuel is extended by about 20% when ilmenite is used as bed

material. The reasons for this delay probably lie within the reaction kinetics of the char combustion as the O_2 partial pressure represents one decisive factor.

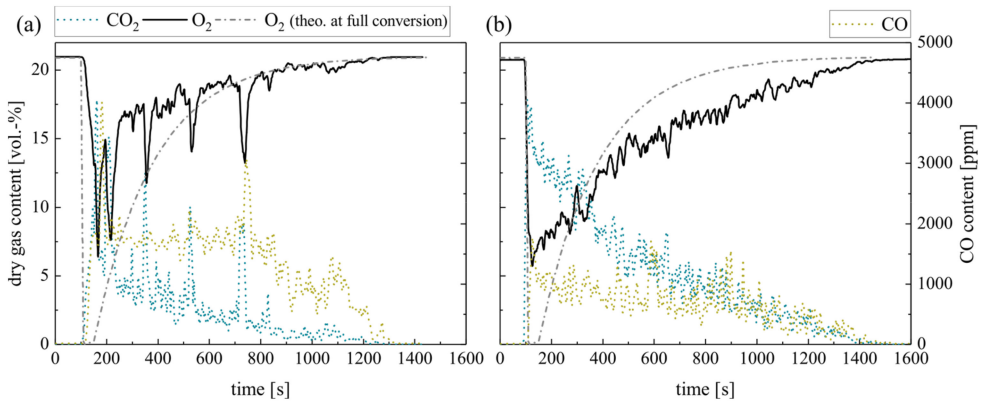

Figure 6. Dry gas composition measured at the fluidized bed surface for (**a**) silica sand and (**b**) ilmenite with char pellets as fuel (measurement series no. 2).

Thus, the authors propose the following mechanism during transient char combustion with an OC: ilmenite favors the oxidation of emerging CO and consequently gets reduced. Subsequently, reduced ilmenite particles react again with gaseous oxygen. Hence, the oxygen partial pressure in the BFB decreases locally. As char oxidation is mainly a mass diffusion-limited process, the lower oxygen content in the atmosphere directly affects the char conversion in the BFB. Due to these competing gas–solid reactions, the char particles have a longer residence time in the ilmenite fluidized bed until full conversion is achieved. With regard to steady-state combustion processes, this implies that during OCAC, the total char inventory in the bed would increase slightly. This equilibrium inventory raises for a higher oxygen mass provided by the OC and lower overall excess air ratios. Further experiments are necessary to precisely quantify this increase.

4.2. Effect of Ilmenite Transient Wood Pellet Combustion Process

After the separated combustion of volatile matter and solid char, both processes overlay during repeated single and batch wood pellet combustion in the laboratory reactor. The single wood pellet measurements serve to understand the influence during combustion with continuous excess air, while during batch dosage, temporary sub-stoichiometric conditions emerge.

4.2.1. Single Wood Pellet Combustion with Ilmenite

Figure 7 displays the dry gas composition during repeated single wood pellet dosage (0.7 g per pellet every 60 s) in silica sand (a) and ilmenite (b) BFB. The O_2 concentration right above the silica sand BFB indicates very low oxygen consumption. Low CO_2 concentrations confirm the low complete conversion of the solid fuel in the BFB. In contrast, ilmenite enhances the O_2 consumption directly in the BFB. An elevated CO_2 concentration confirms the fuel conversion in the BFB. However, both O_2 profiles differ significantly from the theoretical residual oxygen content at full conversion, as depicted schematically.

Regarding the CO concentrations, a significant difference is evident: low CO concentrations applying ilmenite indicate complete conversion to CO_2, while high CO concentrations emerge using silica sand. Moreover, the CO concentration only decreases approx. 200 s after the last pellet supply. Similarly, the CO_2 and O_2 concentrations take this period to return to the initial composition. The reason for this is the combustion of the remaining accumulated char (max. 1.1 g). Overall, the experiments reveal very low in-bed CO_2 yields, although ilmenite results exceed silica sand values by far (see Table 6). Similarly, ilmenite provides only a minor amount of surplus oxygen (see Table 6) compared to the methane measurements (series no. 1, see Table 5) before.

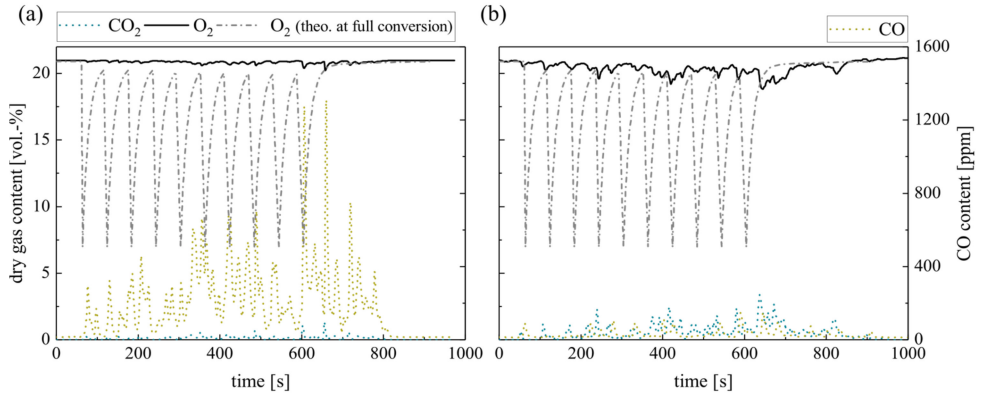

Figure 7. Dry gas composition measured at the fluidized bed surface for (**a**) silica sand and (**b**) ilmenite with single wood pellets (measurement series no. 3).

Table 6. In-bed CO_2-yield γ_{CO2} and specific surplus provided oxygen for silica sand and ilmenite with wood pellets as fuel (measurement series no. 3 and no. 4).

Measurement Series No.	Bed Material	Overall Cycle Excess Air Ratio λ_c (-)	CO_2-Yield γ_{CO2} (%)	Provided O_2 Mass $\dot{m}_{O_2}$ (gO_2/h per $kg_{ilmenite}$)
3	Silica sand	4.1	3.2	-
3	Ilmenite	4.1	18.1	3.6
4	Silica sand	2.9	5.3	-
4	Ilmenite	2.9	29.1	7.0

As the fuel conversion is hardly detectable right above the fluidized bed, Figure 8 shows the gas profiles above the BFB near the reactor outlet (h_m = 330 mm). The transient oxygen consumption in line with the cyclic fuel dosage now becomes more evident. Hence, significant conversion only takes place above the dense bed in the gas phase. However, the pellet location in the BFB is decisive for the residence time of arising volatiles in the fluidized bed. Therefore, and in order to define the influence of the high overall excess air ratios, the authors increased the supplied pellet mass in the following.

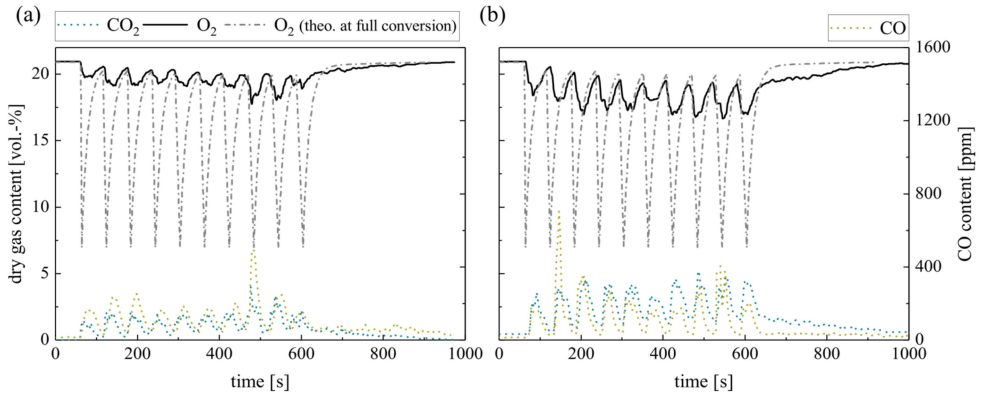

Figure 8. Dry gas composition measured 100 mm above the fluidized bed surface (h_m = 330 mm) for (**a**) silica sand and (**b**) ilmenite with single wood pellets (measurement series no. 3).

4.2.2. Batch Wood Pellet Combustion with Ilmenite

Finally, the repeated batch combustion of 10 g wood pellets in the laboratory reactor concludes the measurements. Figure 9 shows the dry gas composition at the fluidized bed surface for silica sand (a) and ilmenite (b) bed material. The concentrations right above the BFB reveal a similar behavior as during single pellet combustion. However, the O_2 consumption in the fluidized bed increases for both bed materials as the overall excess air ratio decreases. Nevertheless, the difference between the theoretical oxygen

concentration schematically depicted and the measured ones is obvious, especially during the first 40–50 s.

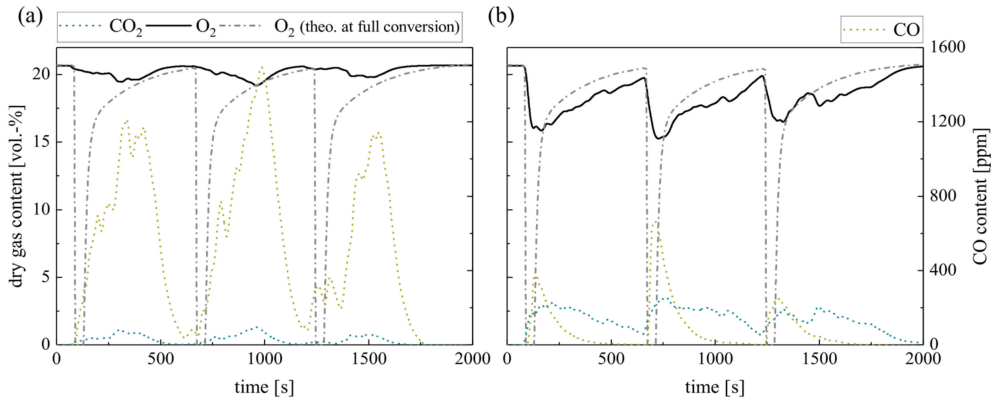

Figure 9. Dry gas composition measured at the fluidized bed surface for (**a**) silica sand and (**b**) ilmenite with batch wood pellets (measurement series no. 4).

Moreover, a general difference between the emerging CO concentrations is evident. Regarding ilmenite measurements, the CO concentration depicts one peak right after the fuel dosage, which is not evident during the single pellet dosage. The sharp CO increase in the beginning results from the temporary sub-stoichiometric conditions, when pyrolysis and devolatilization of the solid fuel take place. During the subsequent char conversion, the CO concentration constantly decreases. On the contrary, the gas profiles during wood pellet combustion in inert silica sand display again an unsteady course, which lasts for the complete combustion process. Again, unsteady flame formation and extinction can be observed on the bed surface.

Besides the difference in the CO concentration, there is an apparent difference in the O_2 profiles. Obviously, the O_2 partial pressure at the BFB surface decreases when applying ilmenite. While in the beginning, during volatile release, the difference exceeds 4 vol.-%, later on, the difference during char conversion still covers approx. 1–2 vol.-%. Due to the low overall conversion during single pellet measurements, this trend was not significant before. This reduction in the oxygen partial pressure prolongs the time until full char conversion. Hence, the O_2 concentration does not return to the initial air concentration in between the batch fuel input.

Further measurements above the BFB near the reactor outlet (h_m = 330 mm) reveal that the gas compositions of silica sand and ilmenite measurements converge (see Figure 10). They indicate a significant oxygen consumption in the freeboard for both bed materials. In particular, silica sand results show that a higher freeboard oxygen conversion balances the lower in-bed oxygen conversion. Thus, the oxygen profiles already align with the theoretical calculated residual oxygen content at full conversion.

This goes along with elevated freeboard CO concentrations right after the fuel input for both materials, although the CO peak is slightly lower for ilmenite. Simultaneously, the CO_2 concentration increases using ilmenite. However, the sharp peaks of unburned species right after the fuel input reveal that ilmenite can buffer these highly sub-stoichiometric conditions only in a limited way. Theoretically, oxidized ilmenite could provide the whole oxygen necessary for the conversion of the wood pellets in the bed. Nevertheless, locally high volatile concentrations emerge around the distributed pellets in the BFB. Moreover, the volatile residence time in the BFB depends on the pellet location. As the density of the wood pellet is lower than the fluidized bed density, the pellets most probably accumulate in the middle to upper part of the BFB. Considering all these limiting factors mitigates the possible enhancement achievable by ilmenite during pyrolysis and volatile combustion. Consequently, the surplus oxygen provided by ilmenite directly in the BFB again decreases (see Table 6) compared to pure methane combustion (see Table 5). The comparison of both pellet measurement series show that the specific provided oxygen increases at lower overall

excess air ratios. This goes along with findings from transient methane combustion (see Figure 4) and steady-state methane combustion processes [18].

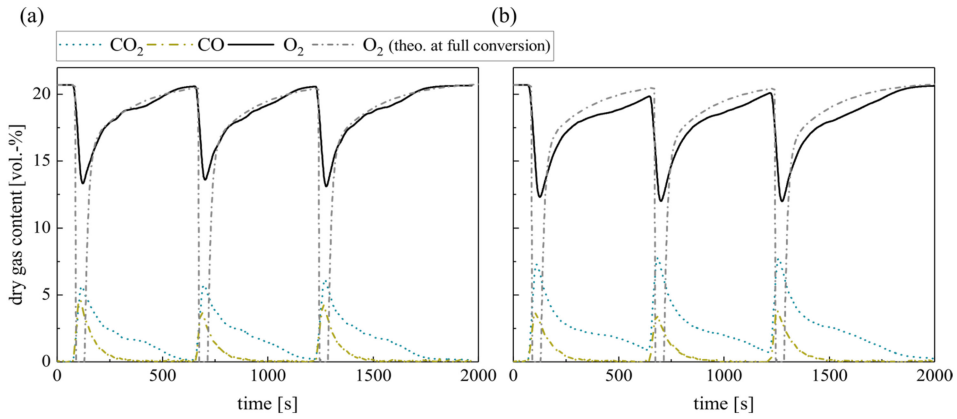

Figure 10. Dry gas composition measured 100 mm above the fluidized bed surface (hm = 330 mm) for (**a**) silica sand and (**b**) ilmenite with batch wood pellets (measurement series no. 4).

4.2.3. Schematic Wood Pellet Combustion during OCAC with Ilmenite

Based on the presented results, the authors conclude that ilmenite has a significant influence on in-bed fuel conversion. In general, the in-bed reacted oxygen increases while a reduction in the CO concentration at the fluidized bed surface and in the freeboard is obvious. However, the enhancing effect mainly concentrates on the volatile conversion at the beginning of the combustion cycle. Subsequently, the re-oxidation of the OC even mitigates the char conversion and extends the overall conversion time.

Based on these correlations, the initial own schematic illustration of the pellet mass and oxygen consumption during wood pellet combustion (see Figure 1) has to be updated for OCAC (see Figure 11). Ilmenite particularly influences the provided oxygen for the combustion process directly in the BFB; the oxygen supply during the temperature-driven pyrolysis increases and enhances the combustion of the volatile matter. However, the amount of surplus provided oxygen highly depends on the excess air ratio, the ilmenite material properties, the overall ilmenite mass and the distribution of the pellets in the bed material. Figure 11 illustrates only the schematic OCAC process based on the experimental results of this research and is not quantified by additional kinetic data.

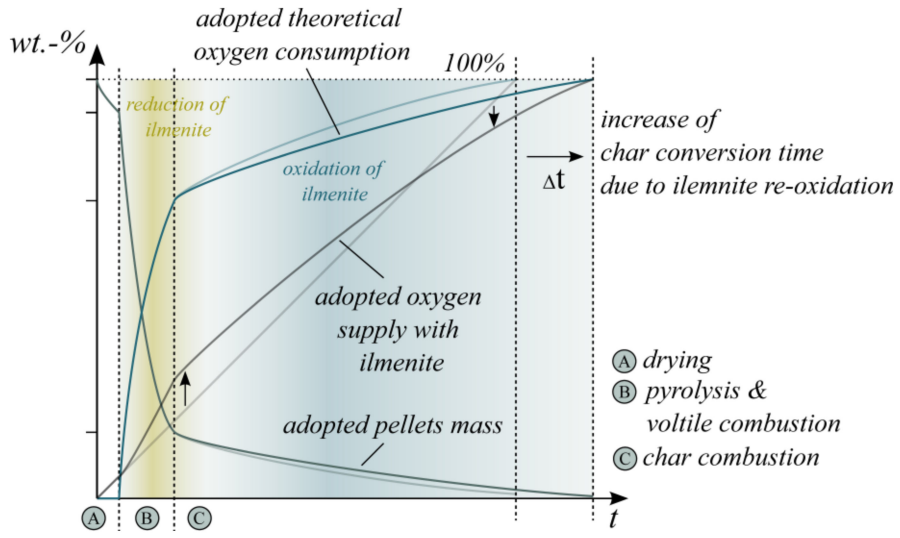

Figure 11. Adopted schematic illustration of the pellet mass, theoretical oxygen consumption and oxygen supply during wood pellet combustion in the presence of ilmenite (OCAC).

From the viewpoint of the OC, the ilmenite reduction is the predominant OC reaction during pyrolysis and the combustion of volatiles. The consequence is a reduced average oxidation state of the OC. Afterward, the oxidation reaction of ilmenite accelerates and achieves the predominant reaction during solid char conversion. The char oxidation is mainly a mass transfer and diffusion-limited process and depends on the partial pressure of the gaseous oxygen. Regarding ilmenite particles, the regime of the oxidation reaction depends on the oxidation state of the OC; highly reduced particles are limited by reaction kinetics. The regime shifts to a diffusion-limited process for highly oxidized particles [52]. Therefore, during the period of char combustion, highly reduced ilmenite particles react with gaseous oxygen first. Thereby, they reduce the oxygen partial pressure at the BFB surface. Consequently, the overall char conversion time expands, as shown before (see Figure 6). Only if the ilmenite particles are oxidized quite completely, both heterogeneous gas–solid reactions become diffusion-limited processes.

Apart from that, ilmenite does not affect the overall oxygen supply for the combustion process during steady-state conditions. As a continuous fuel input results in the continuous overlap of all described combustion steps, the enhancing effect of ilmenite is evident mainly when regarding a higher in-bed fuel conversion and the mitigation of mixing issues [18]. Reduced in-bed CO concentrations are the consequence.

The measured gas profiles in the freeboard area (see Figures 8 and 10) indicate that the CO reducing effect of ilmenite in the BFB can be partially balanced by the post-combustion in the freeboard; a higher oxygen consumption in the gas phase above a silica sand BFB mitigates the measurable effect of ilmenite at the reactor outlet. The overall conversion converges. In order to verify the effect of ilmenite on the continuous combustion of wood pellets, further measurements take place in a 100 kW_{th} BFB unit. There, the focus shifts to the flue gas composition at the reactor outlet.

4.3. Transfer to Continuous Operation with Inhomogeneous Fuel Supply in a 100 kW_{el} BFB Unit

The experiments in a 100 kW_{th} BFB unit enable the investigation of the proposed effects of ilmenite during continuous plant operation but with an inhomogeneous fuel supply. For this purpose, measurements at different overall excess air ratios and fuel input cycle times serve to understand the influence on the CO emissions and the in-bed conversion during homogeneous and inhomogeneous fuel supply at the reactor outlet.

4.3.1. Reduction of the CO Emissions at Transient Fuel Input

In order to clarify the method, Figure 12 shows the exemplary CO concentration profiles at the reactor outlet using silica sand and ilmenite at an overall excess air ratio of $\lambda = 1.5$. The fluctuation in the CO concentrations goes along with the transient fuel dosage starting every 40 s for approx. 10 s. The O_2 and CO_2 concentrations fluctuate in a similar manner. However, the depicted comparison of silica sand and ilmenite measurements already reveals that the absolute CO concentration and the fluctuations are lower using ilmenite. The same counts for the variance of the O_2 concentration, i.e., the oxygen content in the flue gas is smoothened using ilmenite.

Further variations of the fuel input cycle time and excess air ratio confirm this trend. Table 7 summarizes the averaged CO emissions in the flue gas at the reactor outlet depending on the fuel input cycle time. First, it is obvious that the CO emissions highly increase at longer cycle times. This effect is especially enhanced when regarding silica sand and at lower overall excess air ratios. Nearly continuous fuel input (short cycle times) results in a comparable range of CO emissions for silica sand and ilmenite. Simultaneously, the influence of the excess air ratio is mitigated. The reason for the low measured CO reduction by ilmenite during continuous operation (see Table 8) is the large freeboard area of the reactor. Thereby, the residence time of unburnt hydrocarbons extends and further mixing and reaction in the gas phase take place. An increased burnout rate, for silica sand too, is the consequence. The wood pellet batch experiments confirmed this behavior.

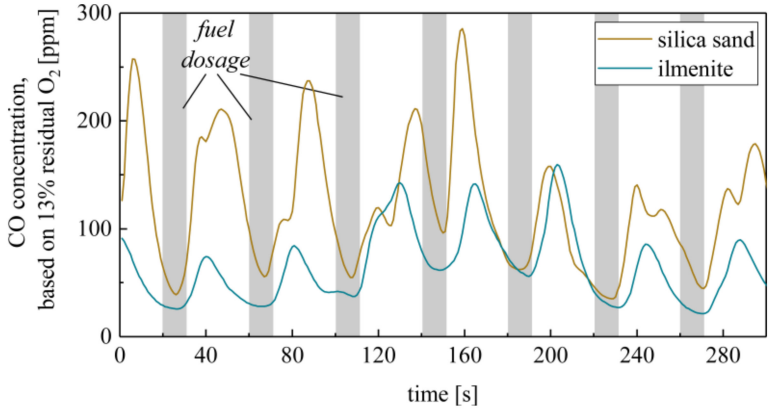

Figure 12. Exemplary CO concentration in the flue gas during transient fuel dosage during silica sand and ilmenite measurements (800°, λc = 1.5 and fuel input cycle time = 40 s).

Table 7. Measured CO emissions and standard deviation in the dry flue gas at varying fuel input cycle times for silica sand and ilmenite depending on the excess air ratio λ.

Cycle Time (s)	Bed Material	CO Emissions Including ± Standard Deviation (ppm)							
		λ_c = 1.3		λ_c = 1.5		λ_c = 1.7		λ_c = 2.0	
5	Silica sand	175.5	±267.0	103.0	±83.0	80.4	±26.0	104.7	±44.3
	Ilmenite	185.9	±188.6	75.5	±37.2	74.7	±28.9	95.8	±40.3
20	Silica sand	161.2	±177.5	107.6	±61.1	90.7	±33.2	144.0	±55.9
	Ilmenite	149.2	±77.6	100.5	±74.7	85.0	±59.2	100.4	±42.9
40	Silica sand	336.8	±631.7	139.5	±202.9	112.0	±57.5	109.8	±62.5
	Ilmenite	301.4	±325.8	99.1	±59.1	88.5	±75.2	69.9	±47.3
60	Silica sand	1796.5	±2002.8	587.8	±755.3	269.1	±454.6	142.1	±95.8
	Ilmenite	1358.3	±1768.3	153.9	±230.8	118.4	±97.3	75.4	±67.0

Table 8. Reduction of the CO emissions in the dry flue gas by ilmenite at varying fuel input cycle times and excess air ratios.

Cycle Time (s)	Reduction of CO Emissions (%)			
	λ_c = 1.3	λ_c = 1.5	λ_c = 1.7	λ_c = 2.0
5	−5.9	26.7	7.0	8.6
20	7.4	6.6	6.2	30.3
40	10.5	29.0	21.0	36.3
60	24.4	73.8	56.0	46.9

The authors examined the reduction potential of the CO emissions by ilmenite during continuous combustion processes before [15]. The results obtained from a small-scale BFB pilot plant demonstrated a CO reduction potential of up to 75%. The reduction was maximized at poor combustion conditions, i.e., relatively low fluidized bed temperatures (750 °C). Hence, the reduction potential highly depends on the reactor geometry and operation conditions. Increasingly transient fuel input results in poor combustion conditions. Thus, the enhancing effect of ilmenite becomes more significant at transient fuel inputs. The highest CO reduction (73.8%) is achieved at an overall excess air ratio of 1.5 and fuel input cycle time of 60 s (see Table 8). The depicted standard deviation of the measurement values confirms that the fluctuations in the CO emissions decrease likewise for ilmenite (see Table 7). However, further reduction in the excess air ratio results in an increasing CO content in the flue gas as highly sub-stoichiometric conditions become predominant.

According to the results obtained from the batch experiments, ilmenite mainly affects the volatile combustion and enhances sub-stoichiometric conditions temporarily. The sharp increase in the CO content between 40 and 60 s cycle times correlates exactly with the

pyrolysis and volatile combustion time periods; while the pyrolysis is not yet complete after 40 s, almost complete conversion of the volatiles takes place after 60 s. This results in oxygen-rich conditions right before the next fuel input starts and sub-stoichiometric conditions right after the fuel input. Consequently, there are high fluctuations in the flue gas composition.

Theoretically, ilmenite can buffer these conditions by providing surplus oxygen locally and temporarily. The experiments confirm that this buffering ability is limited in reality: the volatile release around the pellets leads to high local volatile concentrations in the upper area of the BFB. Therefore, the proportion of ilmenite, which can provide oxygen, decreases at a higher overall ilmenite mass. Lower bed heights and high surface areas could raise this proportion. Moreover, fuel dosage directly into the BFB would probably enhance the residence time of the volatiles.

4.3.2. Increase in the In-Bed Fuel Conversion

Finally, the batch experiments reveal an increase in the in-bed CO_2 yield, which goes along with higher in-bed fuel conversion. The measurements in the 100 kW_{th} BFB unit confirm the batch experiments so far. As the flue gas composition was measured only at the reactor outlet, the determination of the in-bed CO_2 yield was not possible for this setup. However, higher in-bed heat release would also reflect higher in-bed fuel conversions.

The direct comparison reveals that the necessary electrical heating power to regulate the fluidized bed to 800 °C decreases for ilmenite, while the fuel input and the electrical air preheating remain constant. However, a determination of the absolute heat release in the BFB becomes imprecise by the comprehensive losses and measurement uncertainties. Therefore, Müller et al. [53] proposed a methodology in order to determine the heat release in a BFB more precisely. The first measurements with a small proportion of another ilmenite ore already revealed an increase in the heat release by approx. 5–15% [51]. To confirm and quantify this behavior for the present natural ilmenite, the authors propose subsequent specific measurements for the determination of the in-bed heat release.

5. Conclusions

The experimental measurements reveal that ilmenite affects the thermochemical conversion of woody biomass in a manifold manner. However, the combustion of volatiles is the process step with major influence. During transient combustion of gaseous fuels, ilmenite increases the in-bed fuel conversion significantly. Regarding this, the temporal buffering effect is evident, especially at stoichiometric conditions. In contrast, the specific provided oxygen mass by ilmenite enhances at lower excess air ratios, similar to steady-state conditions.

During subsequent char conversion, ilmenite only reacts with emerging gaseous carbon monoxide, while no solid–solid reaction with the biomass char takes place. At low excess air ratios, the re-oxidation of ilmenite reduces the oxygen partial pressure in the fluidized bed (approx. 1–2 vol.-%) and thereby inhibits the char conversion rate. This extends the overall conversion time, and the char inventory in the BFB is higher during OCAC. The adopted scheme of the combustion process qualitatively summarizes the impact of ilmenite on the oxygen supply and consumption as well as the pellet mass during OCAC. Finally, the measurements in the 100 kW_{th} unit validated the CO reducing effect of ilmenite. The reduction of the CO emissions increases at more transient fuel input. However, the enhancing effect is limited to mild sub-stoichiometric conditions. Hence, ilmenite provides further optimization potentials regarding plant operation, especially for small-scale BFB solutions:

1. The homogenization of the oxygen supply allows the extension of the fuel band toward fuels that are more inhomogeneous, as well as transient fuel input in partial load.
2. The reduction potential of the carbon monoxide emissions allows the reduction in the overall excess air ratios to near-stoichiometric combustion conditions at acceptable emissions. This raises the achievable combustion efficiency.

3. The increase in the in-bed fuel conversion allows a higher heat extraction directly out of the bed. Depending on the plant setup, this potential heat extraction out of the fluidized bed limits the electrical or thermal efficiency of the installed heat sink.

However, the CO reducing effect of ilmenite and the higher in-bed fuel conversion highly depend on the operation parameters and the plant design. Local reducing and oxidizing atmospheres in the reactor, as well as extended residence times of the volatiles in the bed, can improve the effect of the OC. On the contrary, large post-combustion zones above the fluidized bed mitigate the CO reduction and increase in the in-bed fuel conversion by the OC measurable in the flue gas.

Therefore, further experiments in this field are of special interest in order to define the influence of the fluidized bed temperature on the in-bed fuel conversion as well as the CO reducing effect of ilmenite. Moreover, the in-bed char conversion during OCAC processes, especially its observed delay, must be the focus of further detailed research.

Author Contributions: T.S.: Conceptualization, Methodology, Investigation, Validation, Writing—Original Draft Preparation; D.M.: Conceptualization, Supervision, Writing—Review and Editing; J.K.: Supervision, Writing—Review and Editing. All authors have read and agreed to the published version of the manuscript.

Funding: This research received no external funding.

Institutional Review Board Statement: Not applicable.

Informed Consent Statement: Not applicable.

Data Availability Statement: Not applicable.

Conflicts of Interest: The authors declare no conflict of interest.

References

1. Plankenbühler, T.; Müller, D.; Karl, J. Influence of Fine Fuel Particles on Ash Deposition in Industrial-Scale Biomass Combustion: Experiments and Computational Fluid Dynamics Modeling. *Energy Fuels* **2019**, *33*, 5911–5917. [CrossRef]
2. Thunman, H.; Lind, F.; Breitholtz, C.; Berguerand, N.; Seemann, M. Using an oxygen-carrier as bed material for combustion of biomass in a 12-MWth circulating fluidized-bed boiler. *Fuel* **2013**, *113*, 300–309. [CrossRef]
3. Mattisson, T.; Keller, M.; Linderholm, C.; Moldenhauer, P.; Rydén, M.; Leion, H.; Lyngfelt, A. Chemical-looping technologies using circulating fluidized bed systems: Status of development. *Fuel Process. Technol.* **2018**, *172*, 1–12. [CrossRef]
4. Adánez, J.; Abad, A.; Mendiara, T.; Gayán, P.; de Diego, L.F.; García-Labiano, F. Chemical looping combustion of solid fuels. *Prog. Energy Combust. Sci.* **2018**, *65*, 6–66. [CrossRef]
5. Lind, F.; Corcoran, A.; Thunman, H. Validation of the oxygen buffering ability of bed materials used for OCAC in a large scale CFB boiler. *Powder Technol.* **2017**, *316*, 462–468. [CrossRef]
6. Hughes, R.W.; Lu, D.Y.; Symonds, R.T. Improvement of Oxy-FBC Using Oxygen Carriers: Concept and Combustion Performance. *Energy Fuels* **2017**, *31*, 10101–10115. [CrossRef]
7. Moldenhauer, P.; Corcoran, A.; Thunman, H.; Lind, F. A Scale-Up Project for Operating a 115 MWth Biomass-Fired CFB boiler with Oxygen Carriers as Bed Material. In Proceedings of the 5th International Conference on Chemical Looping, Park City, UT, USA, 24–27 September 2018.
8. Rydén, M.; Hanning, M.; Corcoran, A.; Lind, F. Oxygen Carrier Aided Combustion (OCAC) of Wood Chips in a Semi-Commercial Circulating Fluidized Bed Boiler Using Manganese Ore as Bed Material. *Appl. Sci.* **2016**, *6*, 347. [CrossRef]
9. Improbed. Available online: https://www.improbed.com/ (accessed on 11 February 2021).
10. Schneider, T.; Müller, D.; Karl, J. A review of thermochemical biomass conversion combined with Stirling engines for the small-scale cogeneration of heat and power. *Renew. Sustain. Energy Rev.* **2020**, *134*, 110288. [CrossRef]
11. Schneider, T.; Ruf, F.; Müller, D.; Karl, J. Performance of a fluidized bed-fired Stirling engine as micro-scale combined heat and power system on wood pellets. *Appl. Therm. Eng.* **2021**, *189*, 116712. [CrossRef]
12. Gaderer, M.; Gallmetzer, G.; Spliethoff, H. Biomass fired hot air gas turbine with fluidized bed combustion. *Appl. Therm. Eng.* **2010**, *30*, 1594–1600. [CrossRef]
13. Marra, F.S.; Miccio, F.; Solimene, R.; Urciuolo, M.; Chirone, R.; Continillo, G.; Lombardi, S.; Fusco, G. Setup of an integrated Stirling Engine-Fluidized Bed (SE-FB) experimental system. In Proceedings of the 16th International Stirling Engine Conference, Bilbao, Spain, 24–26 September 2014; pp. 24–26.
14. Cuadrat, A.; Abad, A.; Adánez, J.; de Diego, L.F.; García-Labiano, F.; Gayán, P. Behavior of ilmenite as oxygen carrier in chemical-looping combustion. *Fuel Process. Technol.* **2012**, *94*, 101–112. [CrossRef]

15. Schneider, T.; Moffitt, J.; Volz, N.; Müller, D.; Karl, J. Long-term effects of ilmenite on a micro-scale bubbling fluidized bed combined heat and power pilot plant for oxygen carrier aided combustion of wood. *Appl. Energy* **2022**, *314*, 118953. [CrossRef]
16. Lu, D.; de las Obras, M.; Hughes, R. OCAC Using Canadian Ilmenite Ore in a Circulating Fluidized Bed Combustor. In Proceedings of the 80th IEA FBC TCP Spring Meeting, Virtual, 16–17 June 2020.
17. Garcia, E.; Liu, H. Ilmenite as alternative bed material for the combustion of coal and biomass blends in a fluidised bed combustor to improve combustion performance and reduce agglomeration tendency. *Energy* **2021**, *239*, 121913. [CrossRef]
18. Schneider, T.; Krumrein, J.; Müller, D.; Karl, J. Investigation of the Oxygen Supply and Distribution in a Bubbling Fluidized Bed by Using Natural Ilmenite for Oxygen Carrier Aided Combustion. *Energy Fuels* **2021**, *35*, 12352–12366. [CrossRef]
19. Pérez-Orozco, R.; Patiño, D.; Porteiro, J.; Cid, N.; Regueiro, A. Influence of the Feeding Rate on the Transient Behavior of a Biomass Combustor. *Chem. Eng. Technol.* **2019**, *42*, 2520–2529. [CrossRef]
20. Khan, A.A.; de Jong, W.; Jansens, P.J.; Spliethoff, H. Biomass combustion in fluidized bed boilers: Potential problems and remedies. *Fuel Process. Technol.* **2009**, *90*, 21–50. [CrossRef]
21. Nussbaumer, T. Combustion and Co-combustion of Biomass: Fundamentals, Technologies, and Primary Measures for Emission Reduction. *Energy Fuels* **2003**, *17*, 1510–1521. [CrossRef]
22. Wang, X.; Kersten, S.R.A.; Prins, W.; van Swaaij., W.P.M. Biomass Pyrolysis in a Fluidized Bed Reactor. Part 2: Experimental Validation of Model Results. *Ind. Eng. Chem. Res.* **2005**, *44*, 8786–8795. [CrossRef]
23. Reschmeier, R.; Roveda, D.; Müller, D.; Karl, J. Pyrolysis kinetics of wood pellets in fluidized beds. *J. Anal. Appl. Pyrolysis* **2014**, *108*, 117–129. [CrossRef]
24. Reschmeier, R. Kinetik der Thermochemischen Konversion von Holzartiger Biomasse in Wirbelschichten. Ph.D. Thesis, Friedrich-Alexander-University Erlangen-Nürnberg, Erlangen, Germany, 25 September 2015.
25. Neves, D.; Thunman, H.; Matos, A.; Tarelho, L.; Gómez-Barea, A. Characterization and prediction of biomass pyrolysis products. *Prog. Energy Combust. Sci.* **2011**, *37*, 611–630. [CrossRef]
26. Vassilev, S.V.; Baxter, D.; Andersen, L.K.; Vassileva, C.G. An overview of the chemical composition of biomass. *Fuel* **2010**, *89*, 913–933. [CrossRef]
27. Kwong, K.Y.; Marek, E.J. Combustion of Biomass in Fluidized Beds: A Review of Key Phenomena and Future Perspectives. *Energy Fuels* **2021**, *35*, 16303–16334. [CrossRef]
28. Scala, F. A new technique for the measurement of the product CO/CO2 ratio at the surface of char particles burning in a fluidized bed. *Proc. Combust. Inst.* **2009**, *32*, 2021–2027. [CrossRef]
29. Dennis, J.S.; Hayhurst, A.N.; Scott, S.A. The combustion of large particles of char in bubbling fluidized beds: The dependence of Sherwood number and the rate of burning on particle diameter. *Combust. Flame* **2006**, *147*, 185–194. [CrossRef]
30. Linjewile, T.M.; Gururajan, V.S.; Agarwal, P.K. The COCO2 product ratio from the combustion of single petroleum coke spheres in an incipiently fluidized bed. *Chem. Eng. Sci.* **1995**, *50*, 1881–1888. [CrossRef]
31. Peterson, C.A.; Brown, R.C. Oxidation kinetics of biochar from woody and herbaceous biomass. *Chem. Eng. J.* **2020**, *401*, 126043. [CrossRef]
32. Phounglamcheik, A.; Wang, L.; Romar, H.; Kienzl, N.; Broström, M.; Ramser, K.; Skreiberg, Ø.; Umeki, K. Effects of Pyrolysis Conditions and Feedstocks on the Properties and Gasification Reactivity of Charcoal from Woodchips. *Energy Fuels* **2020**, *34*, 8353–8365. [CrossRef]
33. Scala, F. Fluidized-Bed Combustion of Single Coal Char Particles: An Analysis of the Burning Rate and of the Primary CO/CO 2 Ratio. *Energy Fuels* **2011**, *25*, 1051–1059. [CrossRef]
34. Sadhukhan, A.K.; Gupta, P.; Saha, R.K. Modeling and experimental studies on single particle coal devolatilization and residual char combustion in fluidized bed. *Fuel* **2011**, *90*, 2132–2141. [CrossRef]
35. Hesketh, R.P.; Davidson, J.F. The effect of volatiles on the combustion of char in a fluidised bed. *Chem. Eng. Sci.* **1991**, *46*, 3101–3113. [CrossRef]
36. Winter, F.; Prah, M.E.; Hofbauer, H. Temperatures in a fuel particle burning in a fluidized bed: The effect of drying, devolatilization, and char combustion. *Combust. Flame* **1997**, *108*, 302–314. [CrossRef]
37. Hupa, M.; Karlström, O.; Vainio, E. Biomass combustion technology development–It is all about chemical details. *Proc. Combust. Inst.* **2017**, *36*, 113–134. [CrossRef]
38. Mason, P.E.; Jones, J.M.; Darvell, L.I.; Williams, A. Gas phase potassium release from a single particle of biomass during high temperature combustion. *Proc. Combust. Inst.* **2017**, *36*, 2207–2215. [CrossRef]
39. Kajnäs, C.; Hedberg, M.; Leion, H. The Effect of Iron- and Manganese-Based Oxygen Carriers as Bed Materials in Oxygen Carrier Aided Combustion. *Energy Technol.* **2019**, *7*, 1900321. [CrossRef]
40. Gyllén, A.; Knutsson, P.; Lind, F.; Thunman, H. Magnetic separation of ilmenite used as oxygen carrier during combustion of biomass and the effect of ash layer buildup on its activity and mechanical strength. *Fuel* **2020**, *269*, 117470. [CrossRef]
41. Wang, P.; Leion, H.; Yang, H. Oxygen-Carrier-Aided Combustion in a Bench-Scale Fluidized Bed. *Energy Fuels* **2017**, *31*, 6463–6471. [CrossRef]
42. Corcoran, A.; Knutsson, P.; Lind, F.; Thunman, H. Mechanism for Migration and Layer Growth of Biomass Ash on Ilmenite Used for Oxygen Carrier Aided Combustion. *Energy Fuels* **2018**, *32*, 8845–8856. [CrossRef]
43. Yu, Z.; Yang, Y.; Yang, S.; Zhang, Q.; Zhao, J.; Fang, Y.; Hao, X.; Guan, G. Iron-based oxygen carriers in chemical looping conversions: A review. *Carbon Resour. Convers.* **2019**, *2*, 23–34. [CrossRef]

44. Cho, P.; Mattisson, T.; Lyngfelt, A. Comparison of iron-, nickel-, copper- and manganese-based oxygen carriers for chemical-looping combustion. *Fuel* **2004**, *83*, 1215–1225. [CrossRef]
45. Siriwardane, R.; Tian, H.; Miller, D.; Richards, G.; Simonyi, T.; Poston, J. Evaluation of reaction mechanism of coal–metal oxide interactions in chemical-looping combustion. *Combust. Flame* **2010**, *157*, 2198–2208. [CrossRef]
46. Mendiara, T.; García-Labiano, F.; Gayán, P.; Abad, A.; de Diego, L.F.; Adánez, J. Evaluation of the use of different coals in Chemical Looping Combustion using a bauxite waste as oxygen carrier. *Fuel* **2013**, *106*, 814–826. [CrossRef]
47. Moldenhauer, P.; Linderholm, C.; Rydén, M.; Lyngfelt, A. Experimental investigation of chemical-looping combustion and chemical-looping gasification of biomass-based fuels using steel converter slag as oxygen carrier. In Proceedings of the International Conference on Negative CO2 Emissions, Gothenburg, Sweden, 14–17 June 2018; pp. 1–17.
48. Geldart, D. Types of gas fluidization. *Powder Technol.* **1973**, *7*, 285–292. [CrossRef]
49. Reschmeier, R.; Karl, J. Experimental study of wood char gasification kinetics in fluidized beds. *Biomass Bioenergy* **2016**, *85*, 288–299. [CrossRef]
50. Rangel, N.; Pinho, C. Kinetic and diffusive data from batch combustion of wood chars in fluidized bed. *Biomass Bioenergy* **2011**, *35*, 4124–4133. [CrossRef]
51. Müller, D. Kleinskalige Wirbelschichtfeuerungen zur Kraft-Wärme-Kopplung mit Stirlingmotoren. Ph.D. Thesis, Friedrich-Alexander-Universität Erlangen-Nürnberg, Erlangen, Germany, 8 February 2018.
52. Abad, A.; Adánez, J.; Cuadrat, A.; García-Labiano, F.; Gayán, P.; de Diego, L.F. Kinetics of redox reactions of ilmenite for chemical-looping combustion. *Chem. Eng. Sci.* **2011**, *66*, 689–702. [CrossRef]
53. Müller, D.; Plankenbühler, T.; Karl, J. A Methodology for Measuring the Heat Release Efficiency in Bubbling Fluidised Bed Combustors. *Energies* **2020**, *13*, 2420. [CrossRef]